Supporting Information

A multi-responsive 3D deformable soft actuator with tunable structural color enabled by the graphene/cholesteric liquid crystal elastomer composite

Yuhan Zhang [a], Baohua Yuan [a], Yingjie Shi [a], Xinyu Chen [c], Zizheng Wang [b], Longxiang He [a], Bingxuan Wang [a], Jiumei Xiao [d], Meina Yu [a], Yanzi Gao [a], Lanying Zhang [b], Cheng Zou *[a], Ruochen Lan *[c], and Huai Yang *[b]

[a] *Beijing Advanced Innovation Center for Materials Genome Engineering, Institute for Advanced Materials and Technology, University of Science and Technology Beijing, Beijing 100083, P. R. China*

[b] *School of Materials Science and Engineering, Peking University, Beijing 1008711, P. R. China*

[c] *College of Chemistry and Materials, Jiangxi Normal University, Nanchang 330022, P. R. China*

[d] *School of Mathematics and Physics, University of Science and Technology Beijing, Beijing 100083, P. R. China*

**Corresponding authors:*
Huai Yang: yanghuai@pku.edu.cn;
Ruochen Lan: lanruochen@pku.edu.cn;
Cheng Zou: zoucheng@ustb.edu.cn

Supplementary Figures

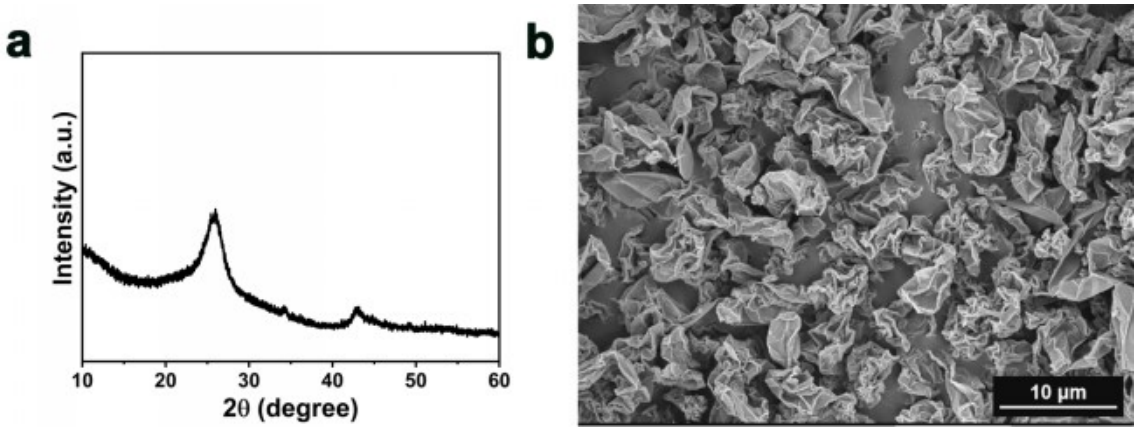

Fig. S1 (a) XRD pattern and (b) SEM image of the RGO powder.

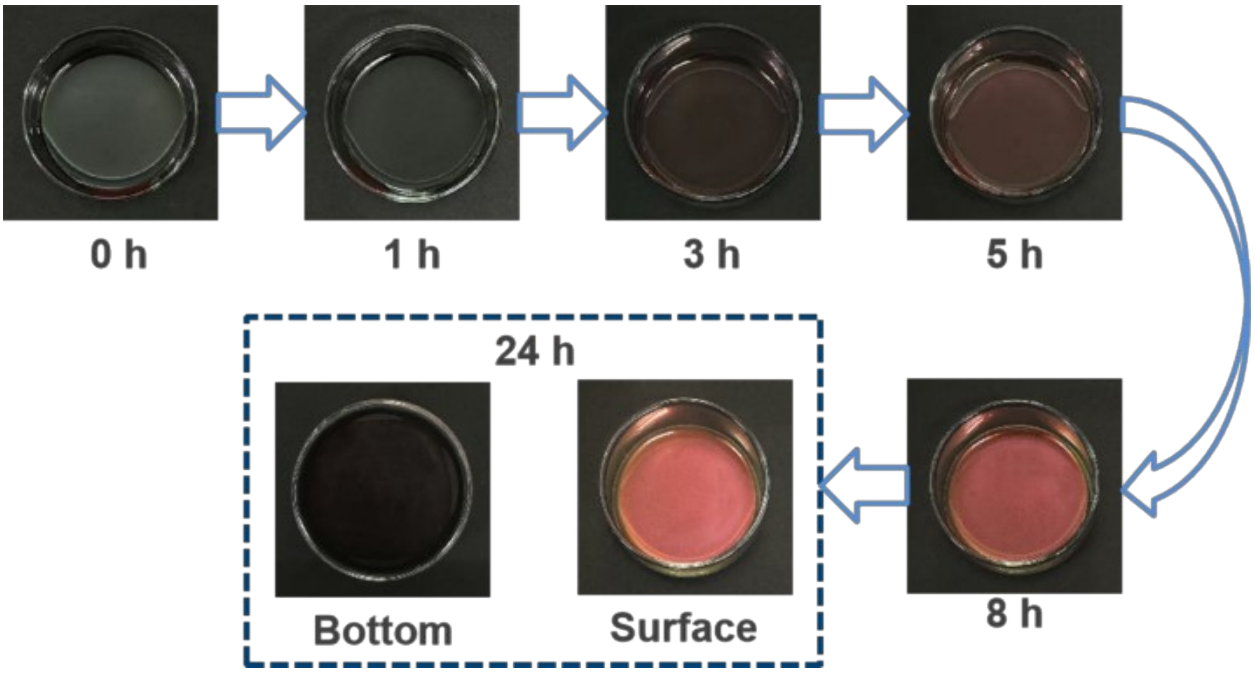

Fig. S2 Photographs of the formation process of the red-reflecting RGO/CLCE film.

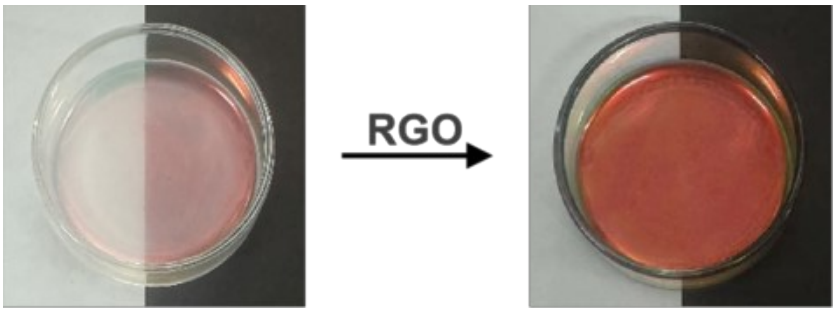

Fig. S3 Photographs of the CLCE film and RGO/CLCE film under light and dark contrast background.

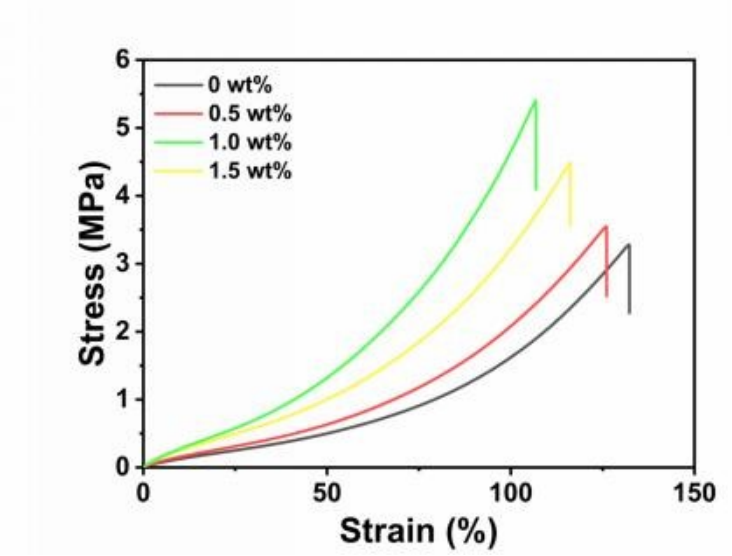

Fig. S4 The stress-strain curves of the RGO/CLCE films with different content of RGO.

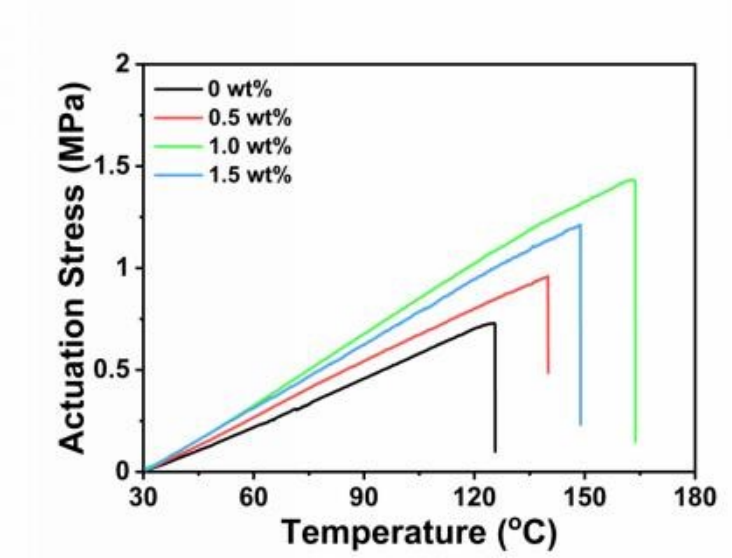

Fig. S5 The actuation stress of the RGO/CLCE films with different content of RGO.

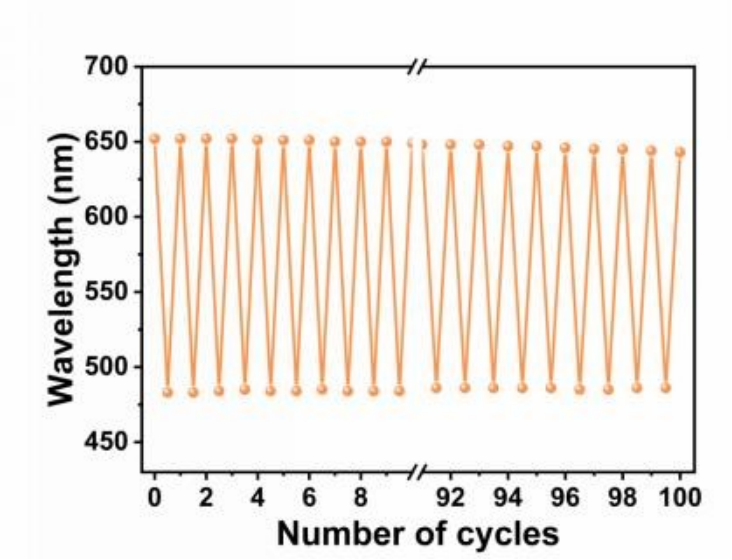

Fig. S6 The reversibility of the mechanical responsive RGO/CLCE film.

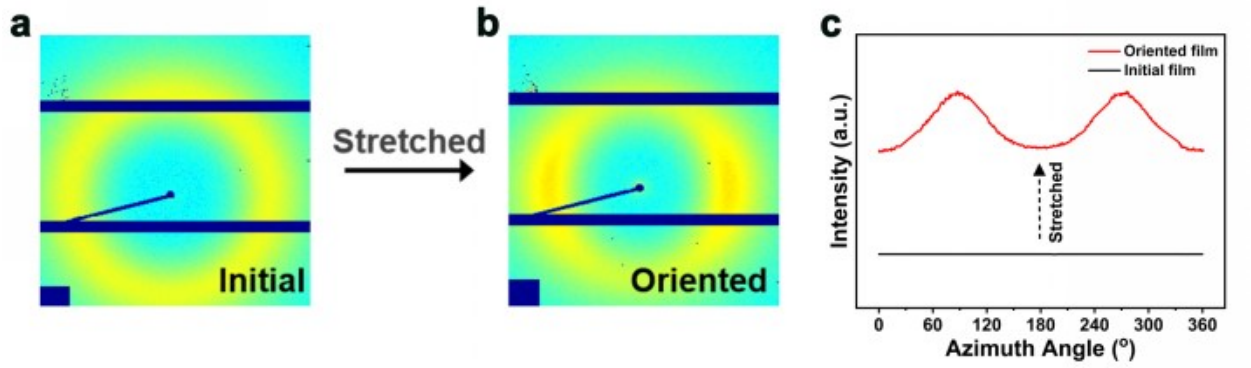

Fig. S7 2D-WAXD patterns of (a) the initial red-reflecting CLCE and (b) the stretched green-reflecting CLCE, (c) 1D azimuthal scanning profiles of the initial red-reflecting CLCE and the stretched green-reflecting CLCE.

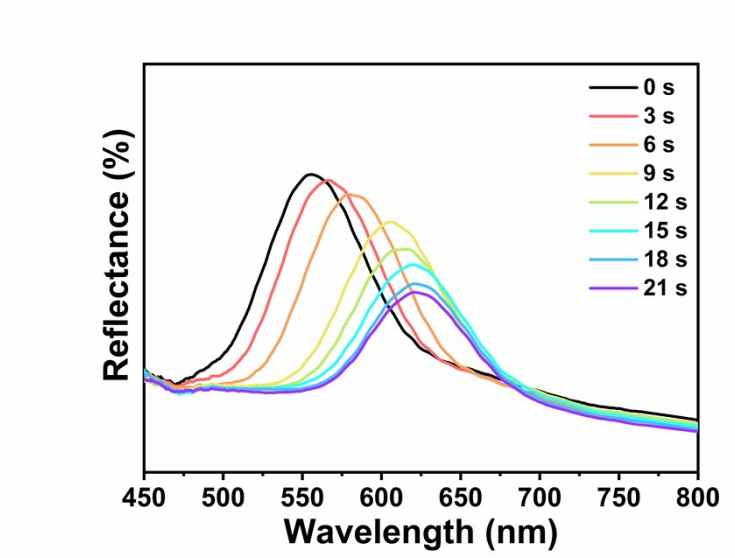

Fig. S8 The reflection spectra of the RGO/CLCE film with different heating times at 120 ℃.

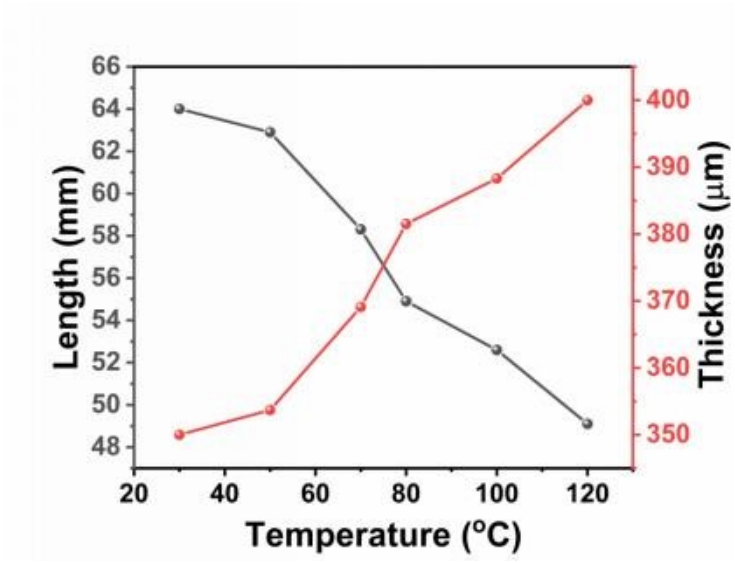

Fig. S9 The length and thickness of the RGO/CLCE film as a function of temperature.

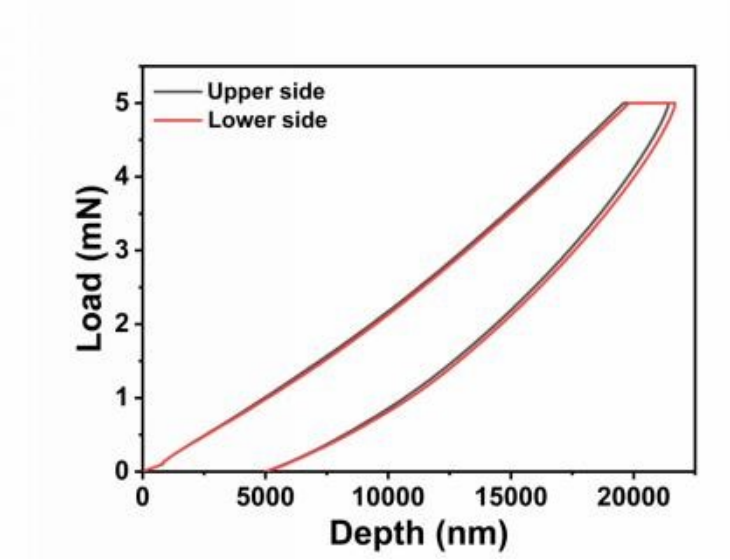

Fig. S10 The load-displacement graphs for the both sides of the CLCE film.

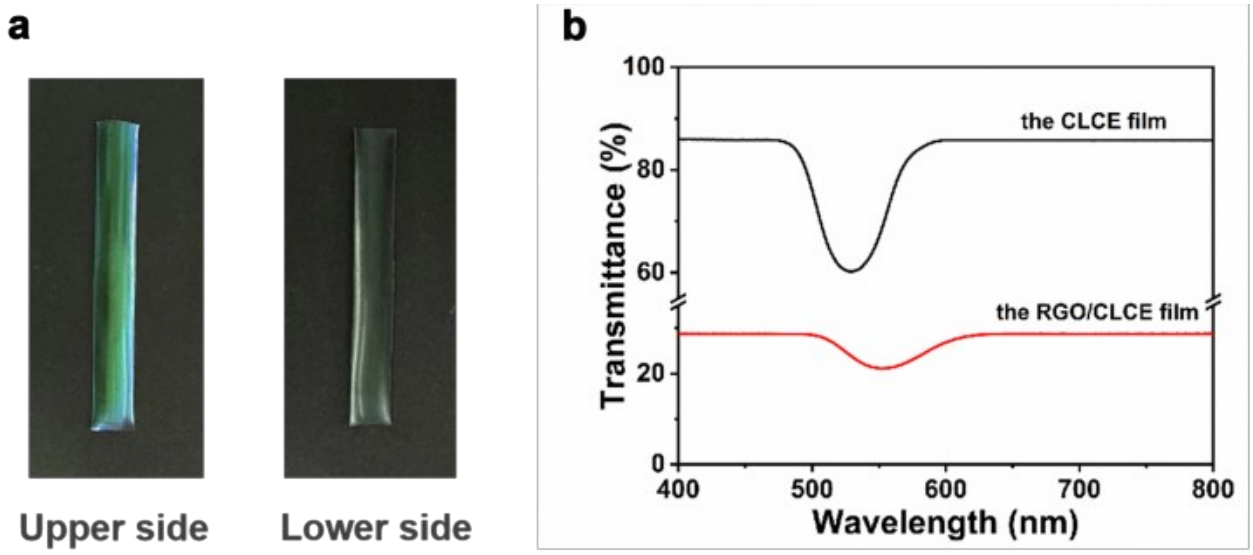

Fig. S11 (a) Photographs of the upper and lower sides of the RGO/CLCE film, and (b) the transmittance spectra of the CLCE film and the RGO/CLCE film.

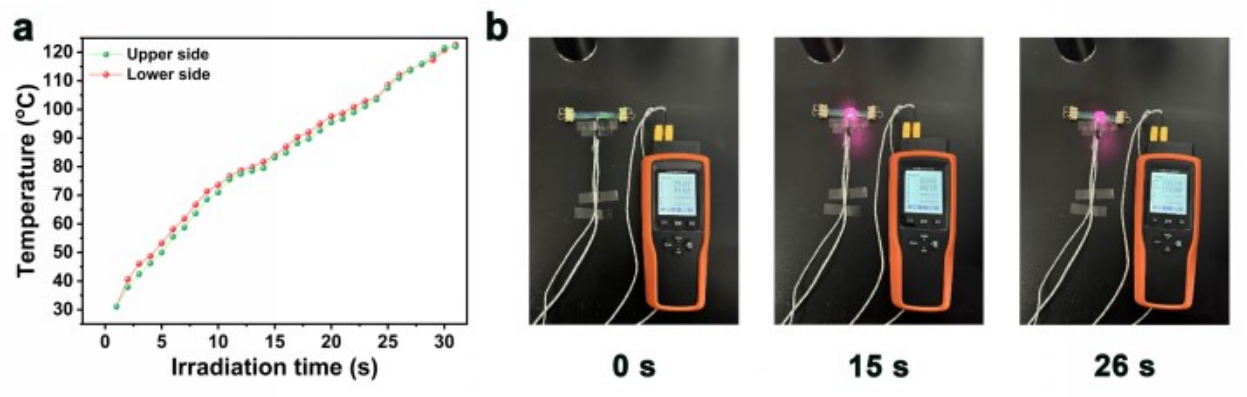

Fig. S12 (a) The temperature of both sides of the RGO/CLCE film as a function of irradiation time, (b) the photographs of thermocouple temperature measurement at different irradiation times.

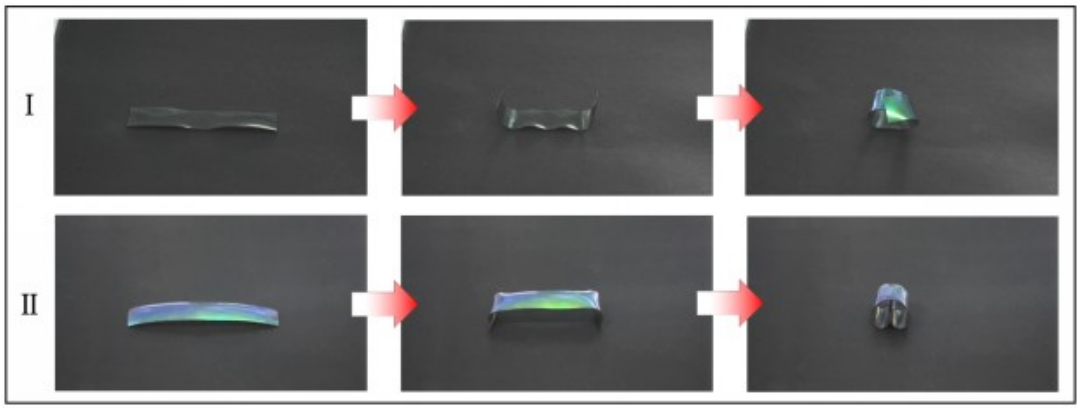

Fig. S13 The thermal deformable photographs of the (I) upper side and (II) lower side.

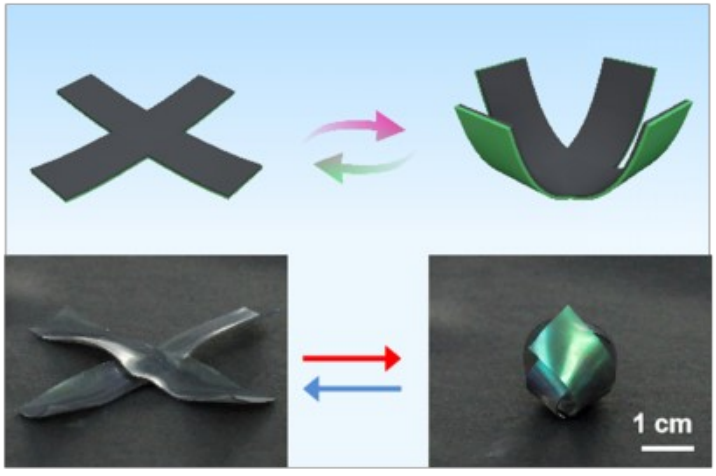

Fig. S14 The schematic illustrations and photographs of the artificial flower structure actuated by thermal stimulation.

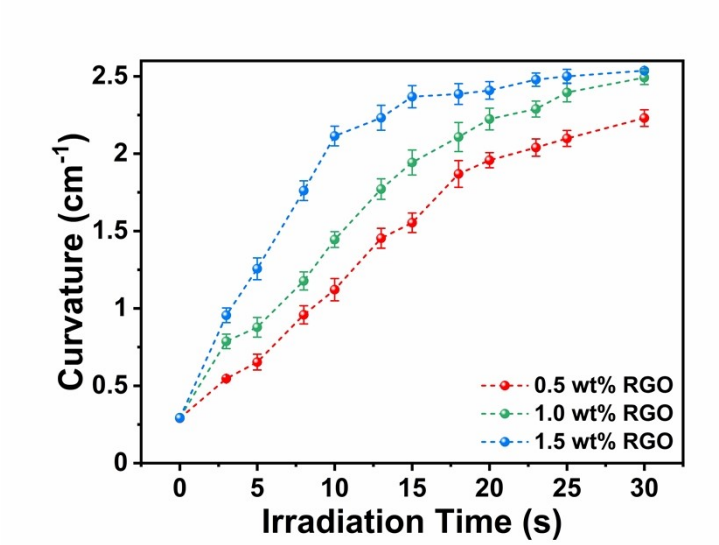

Fig. S15 Curvatures of the RGO/CLCE film with different content of RGO versus irradiation time under NIR light irradiation (irradiation intensity: 1.2 W cm^{-2}).

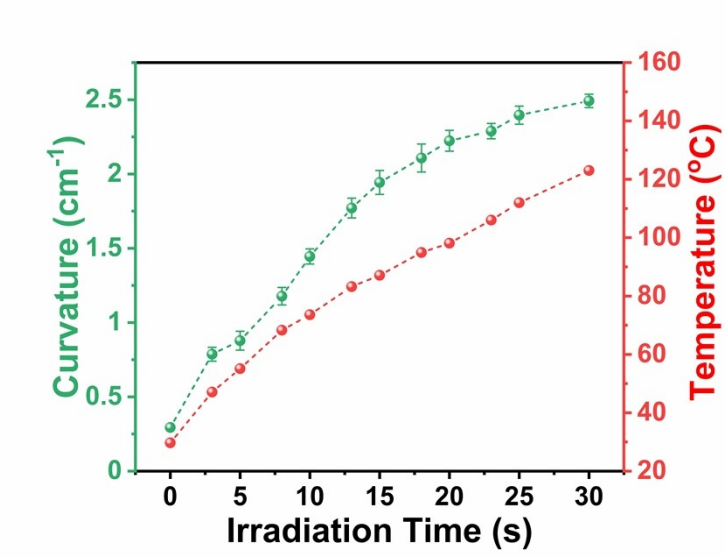

Fig. S16 Curvatures of the 1.0 wt% RGO/CLCE film with NIR light irradiation and its corresponding temperature versus the irradiation time (irradiation intensity: 1.2 W cm^{-2}).

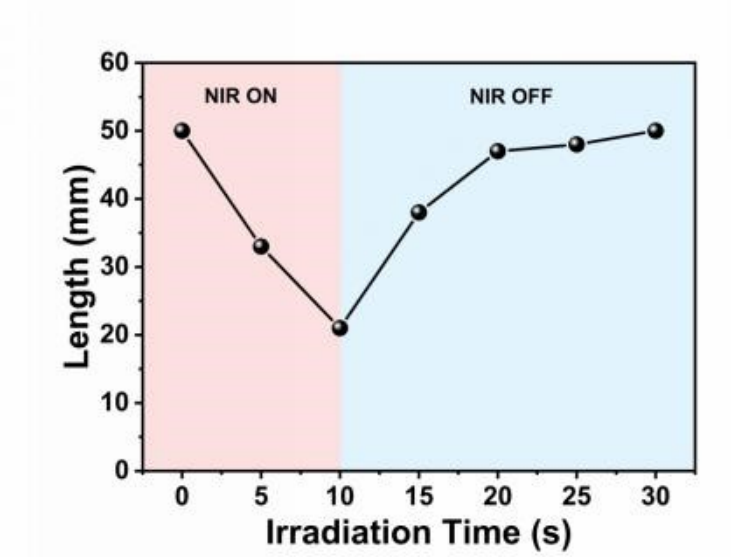

Fig. S17 The length of the RGO/CLCE film as a function of NIR light irradiation time.

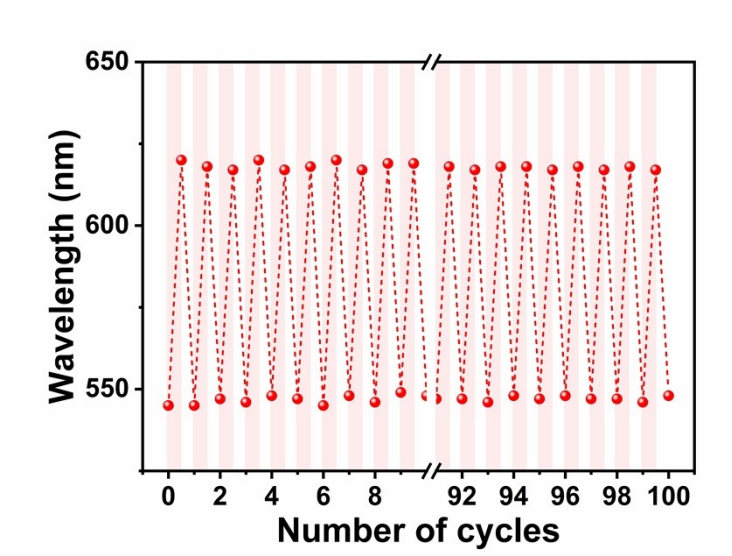

Fig. S18 The reversibility of the reflection spectra of the RGO/CLCE film with NIR light irradiation.

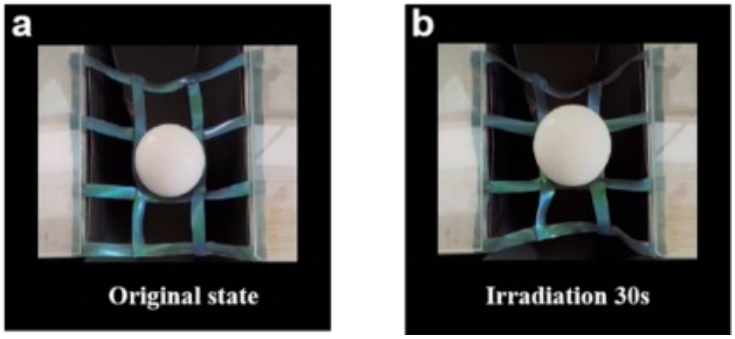

Fig. S19 Photographs of the ball being lifted (a) before and (b) after NIR light actuation.

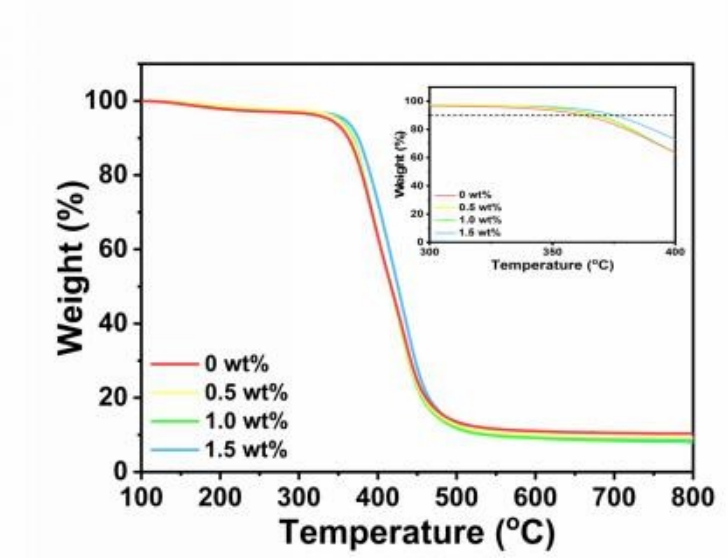

Fig. S20 The TGA curves of the RGO/CLCE films with different content of RGO.

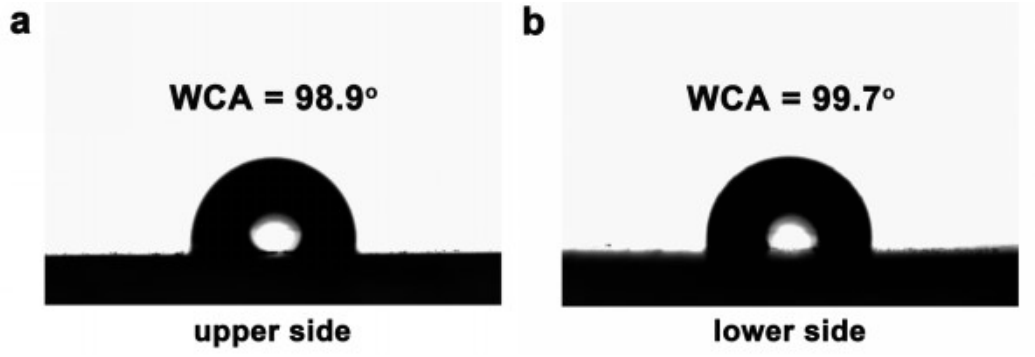

Fig. S21 (a) Images of the water droplet shapes for (a) the upper side and (b) lower side of the RGO/CLCE film, with their respective contact angles.